INAF-Osservatorio astrofisico di Torino
Technical Report nr. 173

Implementation of a CME flag for METIS: first tests

Alessandro Bemporad

Pino Torinese, 15 dicembre 2016

IMPLEMENTATION OF A CME FLAG FOR METIS: FIRST TESTS

A. Bemporad – INAF-Turin Astrophysical Observatory

ABSTRACT

The aim of the analysis reported here is to verify the feasibility of an automatic detection algorithm for major Coronal Mass Ejections (CMEs) with sequences of visible light (VL) data acquired by the Metis coronagraph. After the analysis of not calibrated sequences of unpolarized images acquired by SOHO LASCO-C2, it is shown that, due to the relative weak intensity increase (~ 20%) associated even with strong standard CMEs, the normalization for small possible variations (~ 2%) of exposure times t_i and the removal of spikes will be both crucial in order to automatically identify a CME with simple running differences Δ_i , to be computed as $\Delta_i = (I_{i+1} / t_{i+1} - I_i / t_i)$. Moreover, after the analysis of calibrated sequences of polarized images acquired by STEREO COR1 for a standard and a halo CME, a selection rule is provided for the relative locations of the angular sectors to be used with respect to the orientation of the linear polarizer when Metis will acquire sequences with 4 orientations of the linear polarizer (polarized brightness). This selection rule is required because of the strong polarization of VL emission coming from standard CMEs expanding close to the plane of the sky, making the values of running differences $\Delta_i(\vartheta_n) = I_{i+1}(\vartheta_n) - I_i(\vartheta_n)$ strongly dependent on the considered polarization angle. This effect is less important for halo CMEs expanding away from the plane of the sky, hence weakly polarized. An alternative selection rule for the Metis observations acquired with 2 orientations only of the linear polarizer (total brightness) is also provided. In order to reduce any possible uncertainty associated with the instrument calibration, it is strongly suggested to use the relative (and not absolute) variations of VL running differences $\Delta_i(\vartheta_n)/I_i(\vartheta_n)$ for the definition of a CME signal threshold. Results from first tests reported here show that before the occurrence of CMEs the relative variations of running differences $\Delta_i(\vartheta_n)/I_i(\vartheta_n)$ are very small (on the order of 0.05% in images acquired with single linear polarizer). Hence, during a standard CME a flag should activate when $\Delta_i(\vartheta_n)/I_i(\vartheta_n)$ ~ 0.2%, while for the detection of halo CME a smaller value on the order of $\Delta_i(\vartheta_n)/I_i(\vartheta_n)$ ~ 0.1% will be required.

Summary

List of figures

List of tables

1. Introduction

The aim of the analysis reported here was to verify the feasibility of an automatic detection algorithm for major Coronal Mass Ejections (hereafter CME) with sequences of visible light (VL) data acquired by the Metis coronagraph. The CME flag algorithm should be able at least to perform these three tasks: 1) to rise a first flag ("CME flag") when a major CME enters in the instrument Field of View (FOV), 2) to identify the angular sector of the corona where the CME is centered, and 3) to rise a second flag ("halo flag") when a halo CME occurs.

Each sequence of polarized images acquired by Metis will consist of 4 images with 4 different angular orientations of the linear polarizer with respect to the solar north (0°, 45°, 90° and 135°). No such kind of sequences are available for a test, because existing space based coronagraph acquire polarized images only with 3 different orientations of the linear polarizer (usually 0°, 120° and 240°). In particular for this first analysis sequences acquired by the LASCO-C2 and COR1 coronagraphs onboard the SOHO and STEREO spacecraft (respectively) have been employed. The report is organized as follows: in the first part I describe the LASCO-C2 unpolarized data (§3) and the results obtained concerning possible consequences of exposure time variations (§4.1) and spikes due to cosmic rays (§4.2). In the second part, after a general description of STEREO polarized data (§5), the method of analysis is described (§6), and results obtained for a selected CME (§7) and a halo CME (§8) are shown.

2. Description of the SOHO/LASCO-C2 analyzed data

In order to perform a first "blind" test on the possible implementation of a CME flag I analyzed a sequence of 26 unpolarized images acquired with the "orange" filter by the LASCO-C2 instrument. The data were acquired on August 21, 2001 from 10:27 UT to 19:27 UT, with an average time cadence by about 21.6 minutes and an exposure time on the order of 25 seconds, with small variations (see later); each image has dimensions by 1024x1024 pixels, with a nominal spatial resolution by 11,4 arcsec/pixel. During this sequence of 26 exposures, a standard CME starts to enter in the coronagraph FOV in the 5^{th} frame (12:27 UT), then it propagates above the West limb starting to leave the FOV in the 9^{th} frame (14:06 UT); a sequence of calibrated images is shown in Figure 1.

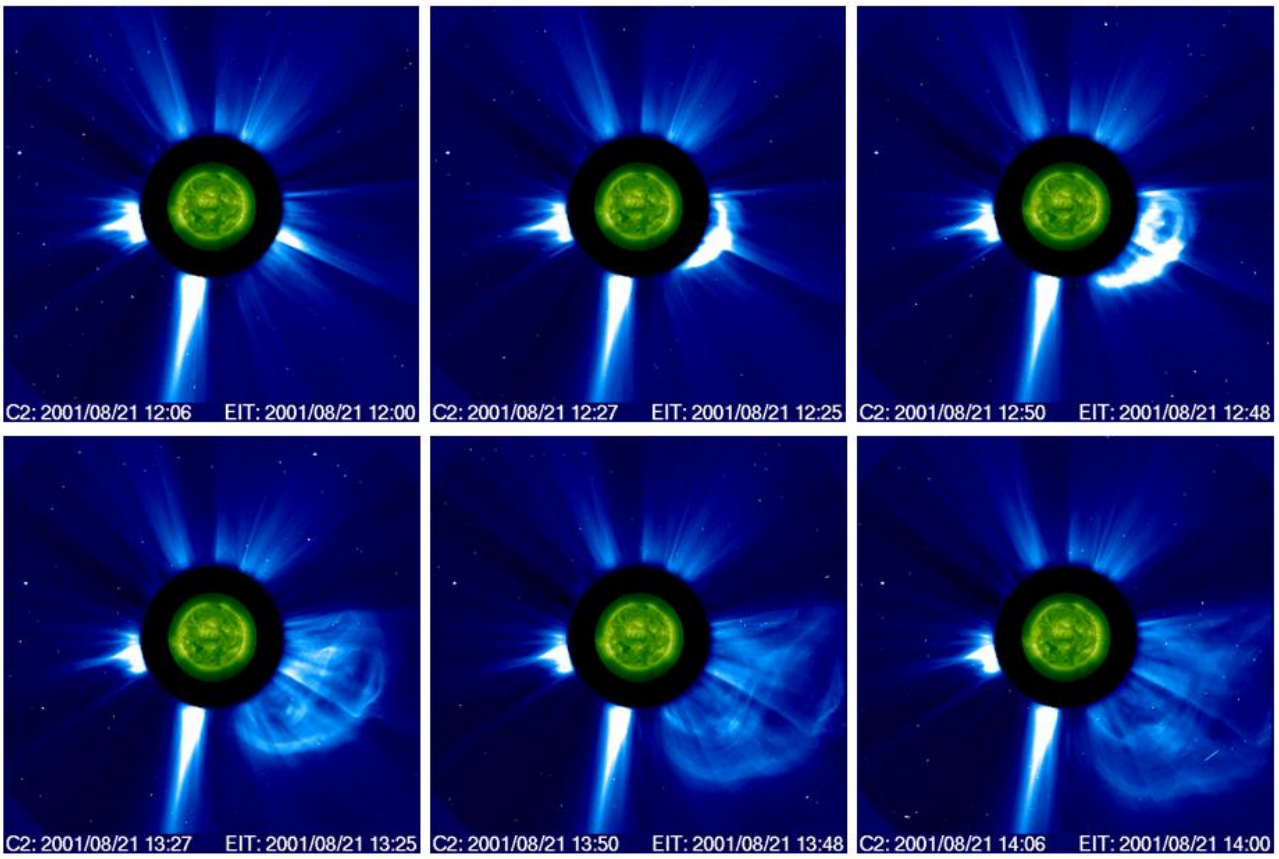

Figure 1: sequence of LASCO-C2 (blue color scale) and EIT 195 (green color scale) images showing the August 21, 2001 CME. These standard sequences available on-line show the intensity variation enhanced with the removal of a monthly-averaged image, but the real absolute variations due to CMEs are quite small (see later).

3. Method of analysis

In order to determine what are the typical visible light intensity variations observed during a CME, and in order to perform a first "blind test" on the implementation of a CME flag, simple running differences were built directly from the LASCO-C2 unpolarized images before data calibration (hence in units of Data Numbers, DNs). In each image the signal goes typically from ~ 4000-4500 DNs close to the inner occulter edge in the brighter structures (coronal streamers) down to around ~ 1000-1500 DNs close to the outer occulter edge in the darker structures (coronal holes). Running differences are built by simple subtraction of uncalibrated exposures, hence the intensity in the *n*-th running difference frame is given in each pixel by the intensity observed in the *n*-th frame minus the intensity observed in the *n-1*-th frame.

3.1 Intensity variations due to different exposure times

The resulting sequence of running differences is shown in Figure 2, with a fixed color scale between -25 DNs and +25 DNs. This Figure clearly shows that:

- significant intensity variations are observed during the CME only in the coronal region crossed by the eruption (after the 5-th frame);

- very strong intensity variations are observed in the whole image before (frame 2) and during (frames 15, 20, 21, 24) the eruption.

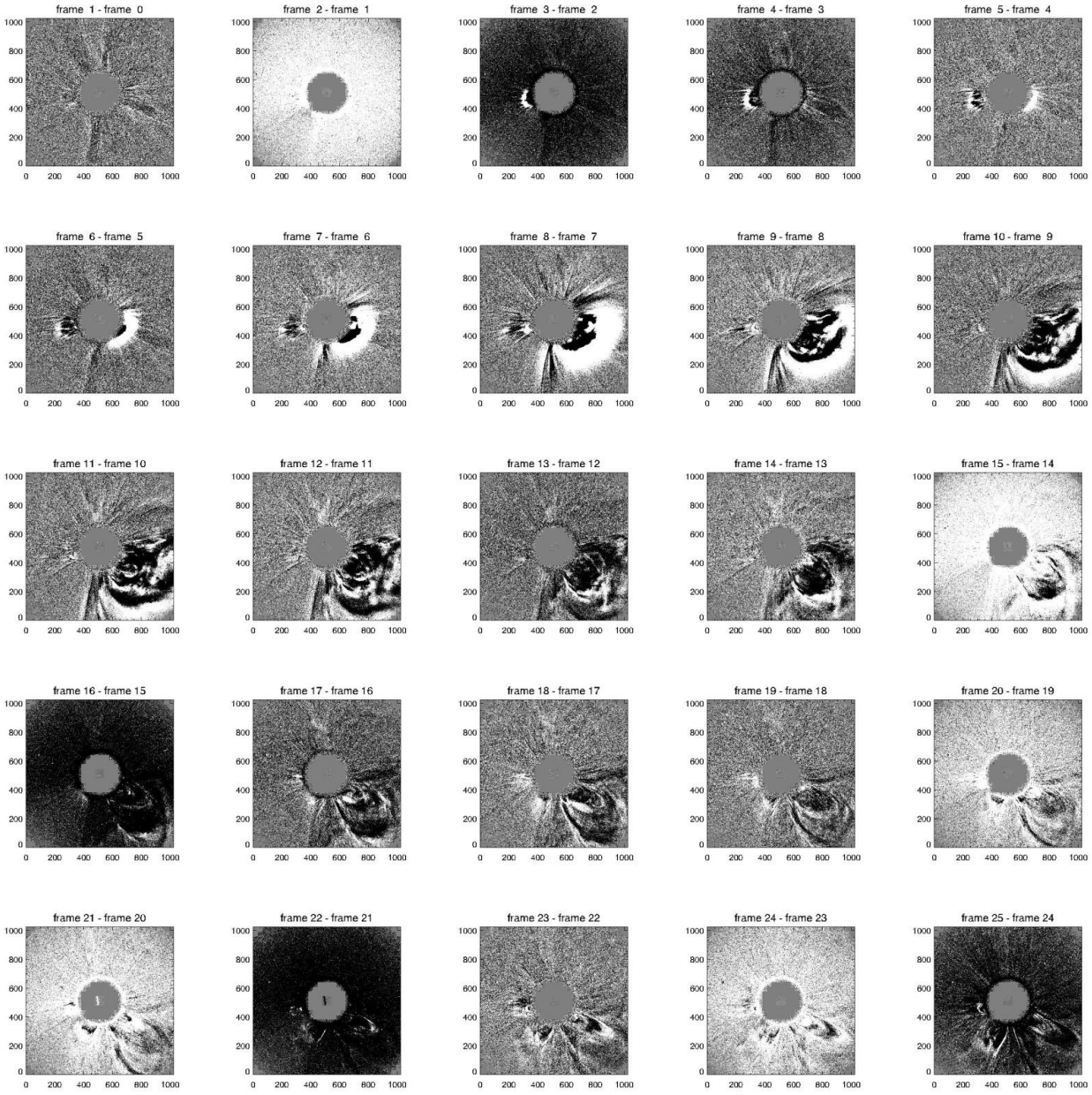

Figure 2: sequence of LASCO-C2 running differences built with uncalibrated exposures (color scale from -25 DNs to +25 DNs).

These strong intensity variations observed in the whole images and shown in Figure 2 are simply due to small variations in the LASCO-C2 exposure time. This important conclusion is demonstrated in Figure 3, showing for different frames (*x*-axis) the exposure times (1st row from the top), the average signal (DNs) over the whole images (2nd row), the intensity standard deviations (3rd row), the average running difference signal (4th row), and the running difference standard deviations (5th row). These plots clearly demonstrate that significant average intensity increases occur not only during the CME (frames 5-14) but also when variations on the order of 0.5 seconds (i.e. about 2% of the exposure time) occur; absolute variations of image intensity due to different exposure times are comparable with or even stronger than

variations due to the CME. The reason is that relative variations due to the CME alone are very small (about 20% for this strong event in the pixel crossed by the CME): when these small variations are averaged over a larger area of the detector including also many detector pixels unaffected by the eruption, the resulting intensity variations become even smaller and comparable with those due to the exposure time variations alone. As a consequence, simple uncalibrated exposures are not suitable for the implementation of an automatic algorithm based on running differences: correction for possible different exposure times will be required.

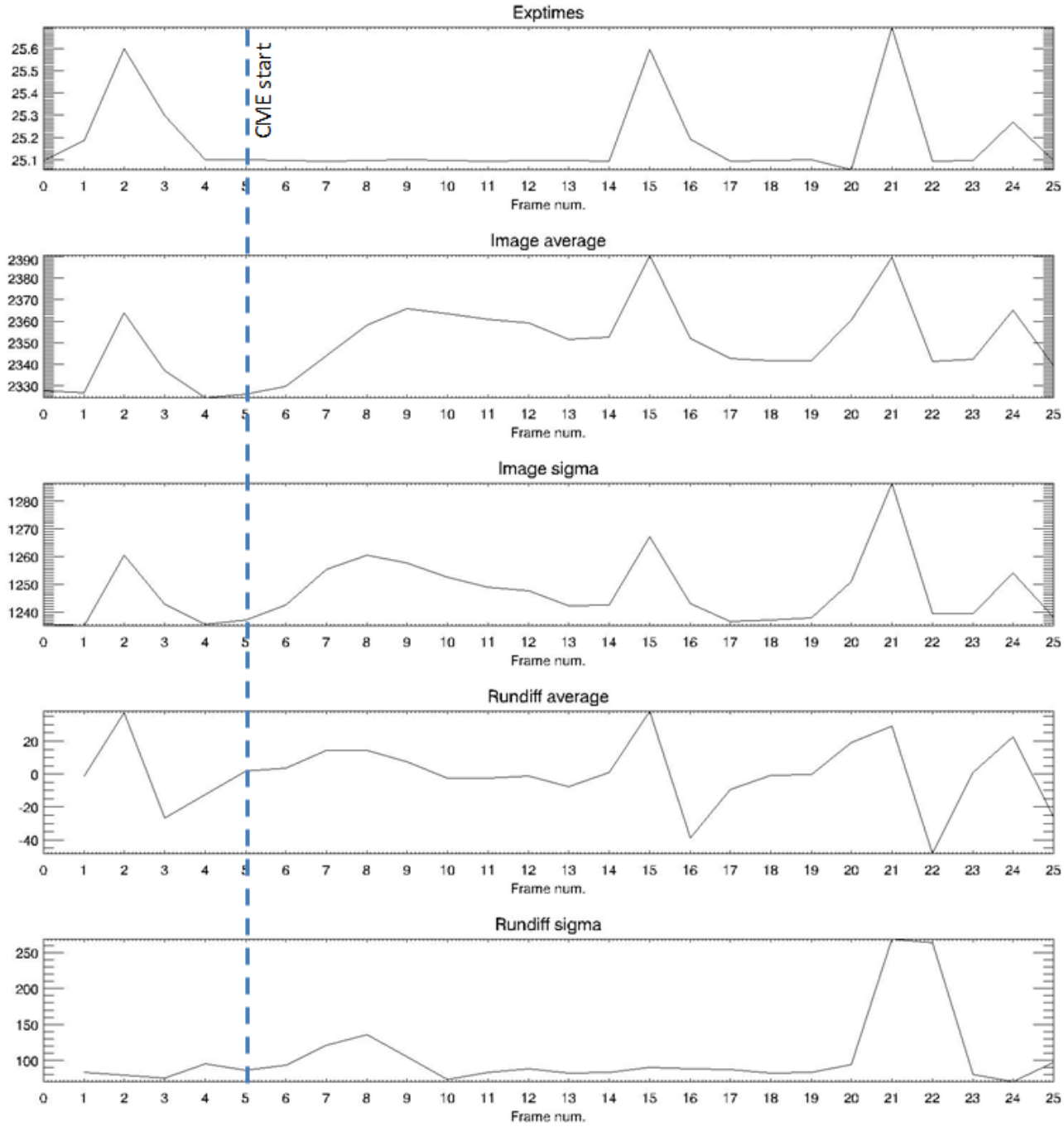

Figure 3: exposure times (1st row from the top), average signal (DNs) over the whole images (2nd row), the intensity standard deviations (3rd row), the average running difference signal (4th row), and the running difference standard deviations (5th row).The vertical dashed line shows the frame corresponding to the first appearance of the CME in the instrument FOV.

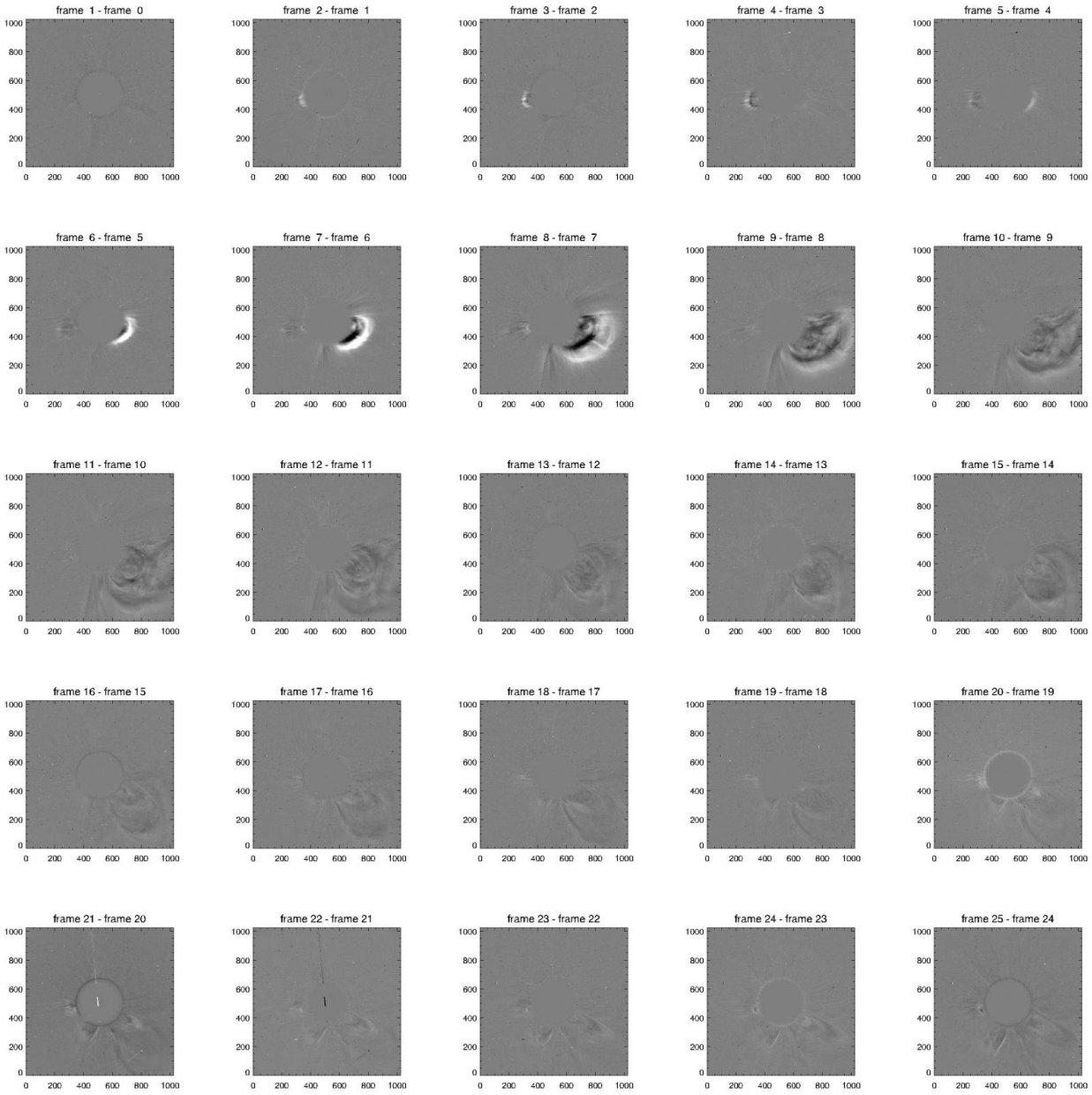

Figure 4: same as Figure 2, after normalization for different exposure times.

The normalization will solve the problem very easily, as it is clearly demonstrated in Figure 4 showing the same sequence of running differences given in Figure 2, with the big difference that each exposure has been divided by the exposure time before the computation of the running difference. Hence sequence of normalized running differences was built as

$$\Delta_i = (I_{i+1}/t_{i+1} - I_i/t_i)$$

where I_i is the intensity (DN) observed in the i-th frame and t_i (seconds) is the corresponding exposure time.

3.2 Intensity variations due to the presence of spikes

The analyzed sequence of 26 exposures also contain a bright spike in frame 21, very well visible in Figure 4 as an almost vertical stripe covering an area of about 300 pixels and located approximately at the center of the image. The analysis of this frame demonstrates that the variations of all parameters due to the presence of the spike (average intensity, average standard deviation, running difference, and running difference standard deviations) are larger in any case than variations due to the CME alone. In fact, LASCO-C2 pixels have a depth by 16 bit, hence the majority of pixels affected by the cosmic ray (with the exclusion of those at the boundary of the affected pixel region) have a signal around 16300 DNs. This value is ~ 4 times larger than the number of DNs usually present in the instrument FOV even in correspondence of the brighter coronal structures (~ 4000-4500 DNs), and more than ~ 20 times larger than the intensity increase due to the CME alone. Even if the extension of the spike is spatially limited with respect to the CME, if the running difference signal that will be analyzed for the CME flag will be computed by averaging over a large number of pixels, it will be really hard to make an automatic distinction between a CME and a cosmic ray. As a consequence, the removal of spikes before the computation of the CME flag will be crucial in order to avoid false detections due to cosmic rays.

The analysis described so far focused only on the uncalibrated LASCO-C2 images acquired with the "orange" filter, hence the images were unpolarized. The reason is that only 2 polarized images per day are usually acquired by LASCO, hence a very few CME polarized observations exist. For this reason, in what follows I describe the further results obtained from the analysis of polarized images acquired by the STEREO/COR1 coronagraph with a much higher frame rate. Moreover, in order to avoid problems explained above due to the different exposure times, the following analysis employs calibrated images.

4. Description of the STEREO/COR1 analyzed data

Polarized images by STEREO/COR1 instrument are acquired in triplets (with polarization angles of 0°, 120° and 240° with respect to the solar north) where every single image is acquired with time interval of 12 seconds, and every triplet is acquired with time interval of 5 minutes. Hence, everyday a total of 864 polarized images are acquired, corresponding to 864/3 = 288 polarization triplets per day. Every image has dimensions of 512x512 pixels, with nominal spatial resolution by 3,7 arcsec/pixel and is acquired with a typical exposure time of ~ 1.7 seconds. For this work 2 eruptive events have been selected starting from the STEREO CME catalog available online (http://cor1.gsfc.nasa.gov/catalog/): the first event (hereafter CME1) is a normal CME that occurred on March 24, 2012, and has been used to perform a test on the CME flag. The second event (hereafter CME2) is a halo CME that occurred on March 5, 2013, and has been used to perform a test on the halo flag.

One of the aims of the present analysis is also to verify whether it is possible on one hand to automatically identify major CMEs, and on the other hand to reject minor solar eruptions (like jets, streamer puffs, streamer detachments, etc…). Hence, for the CME flag a total of 2580 polarized images acquired over 3 days between 2012 March 22 (00:05:00 UT) and March 24 (23:55:18 UT) have been analyzed: during this time interval only one major CME occurred on March 24 around 00:15 UT, but 5 more minor eruptions also occurred (see Figure 5). The major event was associated with a big flare occurring at the West limb as seen by the STEREO-B spacecraft, hence the CME was expanding mainly on the plane of the sky (i.e. perpendicular to the line of sight). For the halo flag a total of 321 polarized images acquired over 12 hours

on 2013 March 5 between 00:05:00 UT and 11:55:24 UT have been analyzed. During this time interval only a strong halo CME was observed: the event (shown in Figure 6) was associated also with a flare and a big prominence eruption occurring from an active region located at the center of the disk as seen by STEREO-B spacecraft, hence the CME was expanding towards the observer (i.e. parallel to the line of sight).

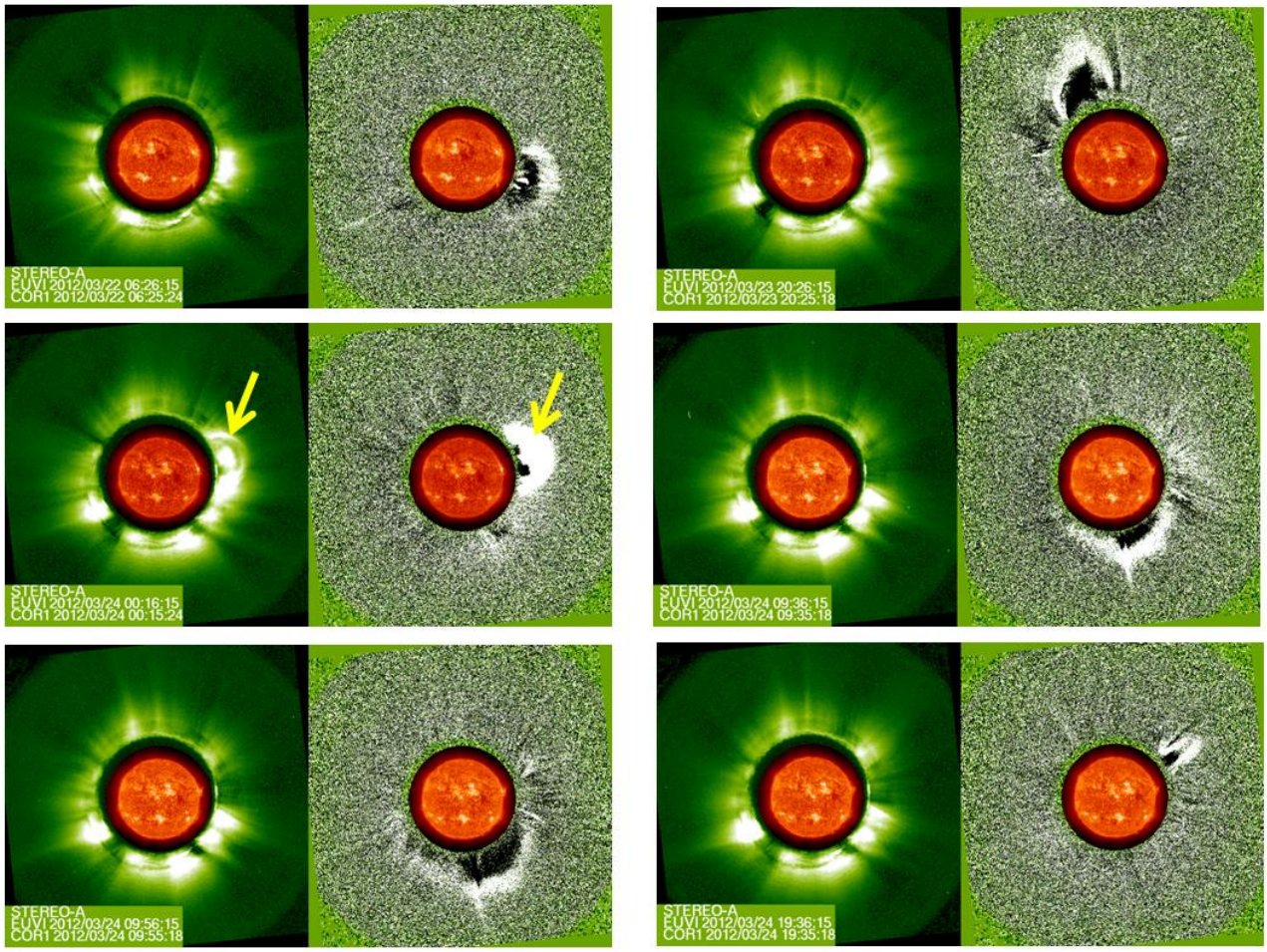

Figure 5: minor and major eruptions occurring in the time interval between March 22-24, each one shown as total (left) and running difference (right) visible light images. The major eruption selected to test the CME flag is shown by a yellow arrow.

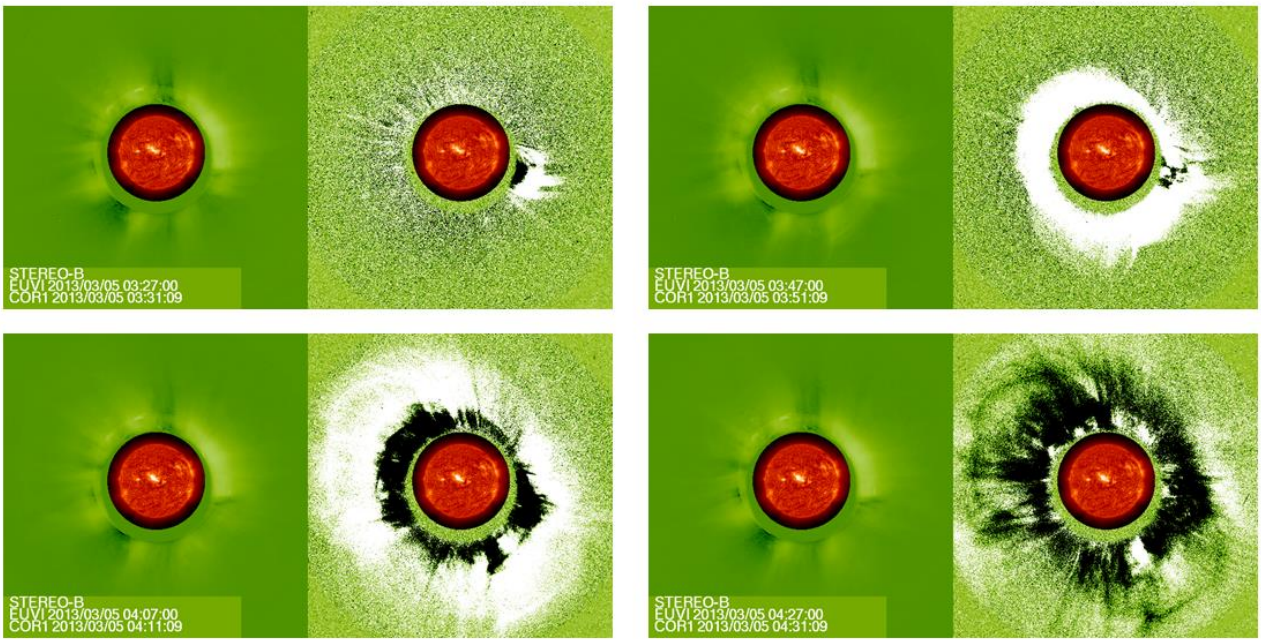

Figure 6: the halo CME (shown as sequence of regular – left – and running difference – right – images) selected to test the halo flag.

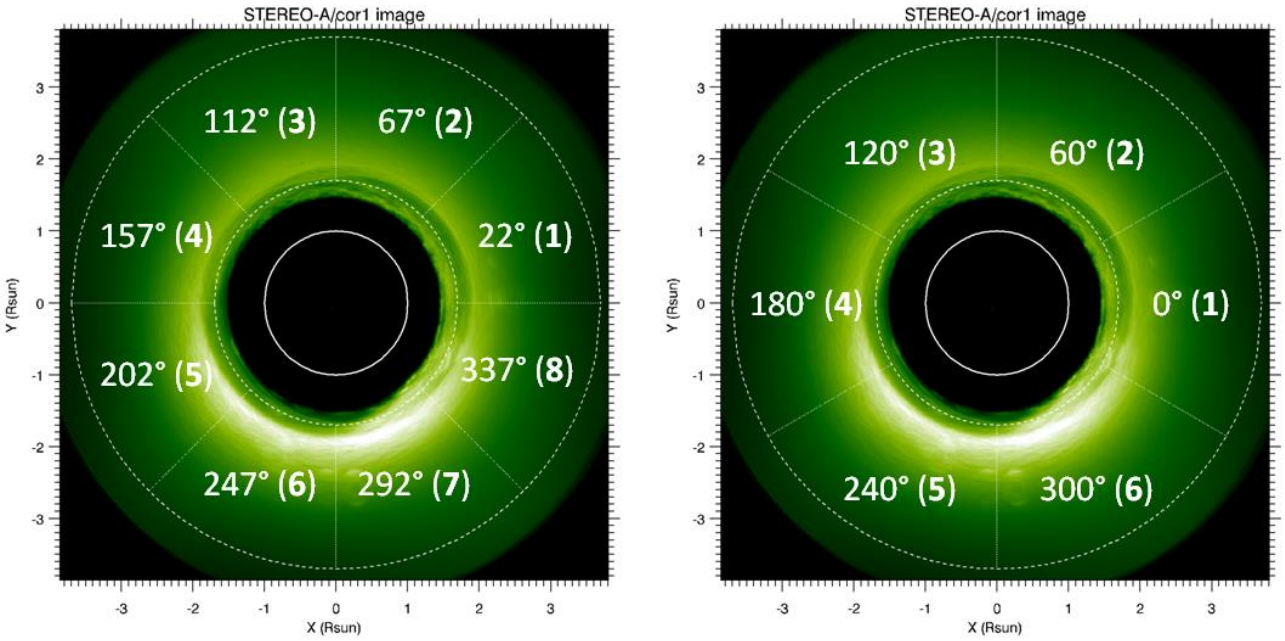

Figure 7, left: location of the 8 angular sectors selected to perform the first test on the CME flag. Right: location of the 6 angular sectors selected to perform the second test on the CME flag. Bold numbers correspond to the identification number of each sector, while degrees refer to the angle (measured counter-clockwise from the solar West) where each sector is centered.

5. Method of analysis

In order to avoid any possible intensity variation due to the different exposure times and isolate the CME emission, each image has been loaded and calibrated in IDL by using the standard routines provided in SolarSoftware within the "Secchi" package (with SCCREADFITS and COR1_CALIBRATE). Moreover, each

triplet of polarized images has been used to derive the total brightness (tB) and polarized brightness (pB) images (with COR1_QUICKPOL). An IDL routine to perform these calibrations and analyses to each one of the images has been written: the routine then extract from every image the intensity averaged over 8 angular sectors, each one with angular extension of 45°, radial extension between 1.7 and 3.7 R_{sun}, with a total number of pixel per sector around ~ 18900 pix. These 8 angular sectors (located starting from the West limb and running counter-clockwise, as shown in Figure 7) cover overall the 57.7% of the total image; in what follows each angular sector is identified with a single number (shown in bold character in Figure 7, left panel) corresponding to the polar angle where the sector is centered: for instance the first sector (1) is centered between 0° and 45° (measured from the West limb), the second sector (2) is centered between 45° and 90°, and so on. The intensity measured over all the pixels located in each one of these sectors has been summed (~18900 pixels per sector) thus producing 8 arrays (one per sector) for the time evolution of the intensity observed in images acquired with a single polarization angle (0°), total brightness (tB) and polarized brightness (pB). These 8 arrays have been derived for 3 kinds of data: 1) intensity observed in the exposures acquired with single orientation (0°) of the linear polarizer, 2) total brightness tB and 3) polarized brightness pB (both computed with the exposures acquired with 3 orientation of the polarizer, 0°, 120° and 240°).

Moreover, for reasons better explained below, the same analysis has been repeated by selecting 6 (instead of 8) angular sectors, each one with angular extension of 60°, radial extension between 1.7 and 3.7 R_{sun}, with a total number of pixel per sector around ~ 21050 pix, centering the first sector over the West limb (see Figure 7, right panel).

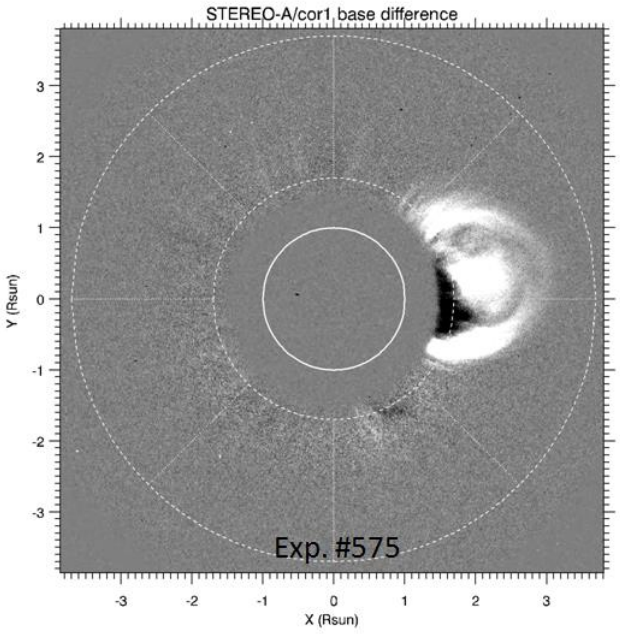

Figure 8: total brightness (pre-CME image subtracted) observed in the exposure (#575) where the CME intensity maximizes, together with the considered 8 angular sectors (dotted lines). This Figure shows that only two angular sectors (#1 and #8; see Figure 7, left panel) were involved in the eruption.

6. Test for a CME flag

As mentioned, the March 24, 2012 CME occurred at the West limb, hence only 2 over the 8 considered angular sectors (#1 and #8) were involved in the eruption (see Figure 8). The intensity evolutions $I_i(\vartheta_n)$

measured for different exposures *i* by averaging over the 8 angular sectors (*n* = 1, 2, … 8) at different angles ϑ are shown in Figure 9 (only for exposures located around the CME). Analysis of resulting evolution clearly shows what follows:

- Days before the major CME:
    - Single polarized exposures (0°) and total VL brightness are almost constant, the 3σ fluctuations over time intervals before the CME are on the order of 0.05%
    - Polarized brightness has a much more significant evolution (fluctuations around 2-3%)
- Hours around the major CME:
    - Single polarized exposures (0 deg) and total VL brightness have a variation by less than 1%
    - Polarized brightness has a variation by more than 20%
    - The stronger variations are observed in angular sectors #1 and #8, hence the angular location of the CME could be easily identified (see below for a better discussion of this point).

The physical explanation for the above results is the following: given the geometry of Thomson scattering, the distribution along the line of sight of the polarized emission is much more concentrated around the plane of the sky, while total brightness is emitted by a much thicker layer of coronal plasma. Hence, for CMEs crossing the plane of the sky (like the one reported here) the bulk of emitting plasma is located around the plane of the sky, hence the resulting increase in the pB emission is relatively much stronger than the increase in the tB. The CME flag algorithm will be developed for the onboard software and will deal with uncalibrated images: hence, a first requirement for this algorithm is to be able to detect variations on the order of 0.5 – 0.7% over a signal with intrinsic fluctuations by less than 0.05%.

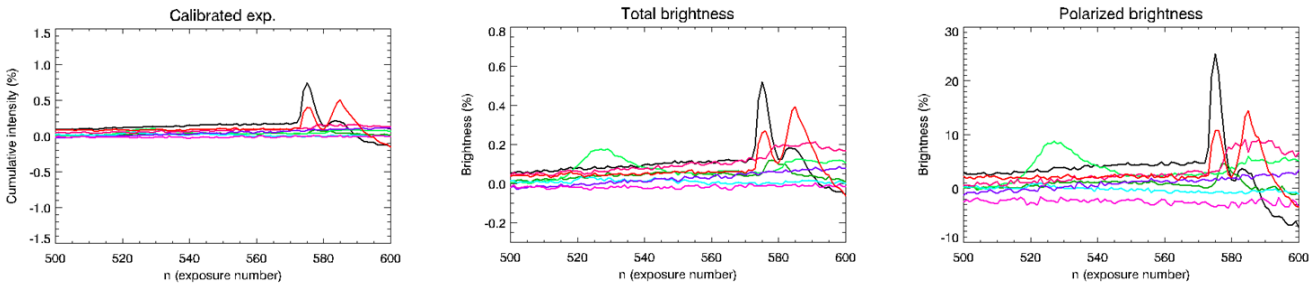

Figure 9: evolution of the intensities (relative variations in %) in different angular sectors (shown with different colors) computed by averaging the signal measured in exposures with single orientation of the linear polarizer (left panel, 0°), total brightness (middle) and polarized brightness (right).

For this first test, running difference signals were also created for each one of the 8 angular sectors: hence (according to what anticipated by previous document on the concept for CME flag algorithm) for each angular sector the quantities $\Delta_i(\vartheta_n) = I_{i+1}(\vartheta_n) - I_i(\vartheta_n)$ have been computed.

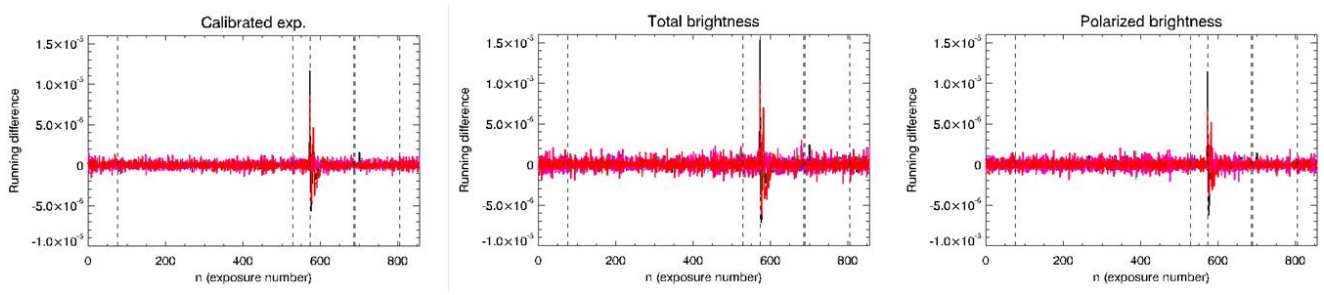

Figure 10: evolution of running difference signals Δ_i over the whole observation interval considered here (3 days of data); different colors represent different angular sectors. Vertical dashed lines show the times when minor eruptions occurred.

Resulting Δ_i values are shown in Figure 10: a significant peak in running differences is visible at the time corresponding to the CME in exposures acquired with single polarization angle (left panel), total brightness tB (middle panel) and polarized brightness pB (right panel). The main results are:

- Running differences allow to unambiguously identify the "big" CME with respect to smaller scale events (Figure 5) which are filtered.
- Running differences are a fast and quick proxy for the determination of CME arrival time (significant increase of running difference already 3 exposures before the CME intensity peak exposure, i.e. 15 minutes before).
- Running difference peak values are comparable for single polarized exposures, tB and pB.

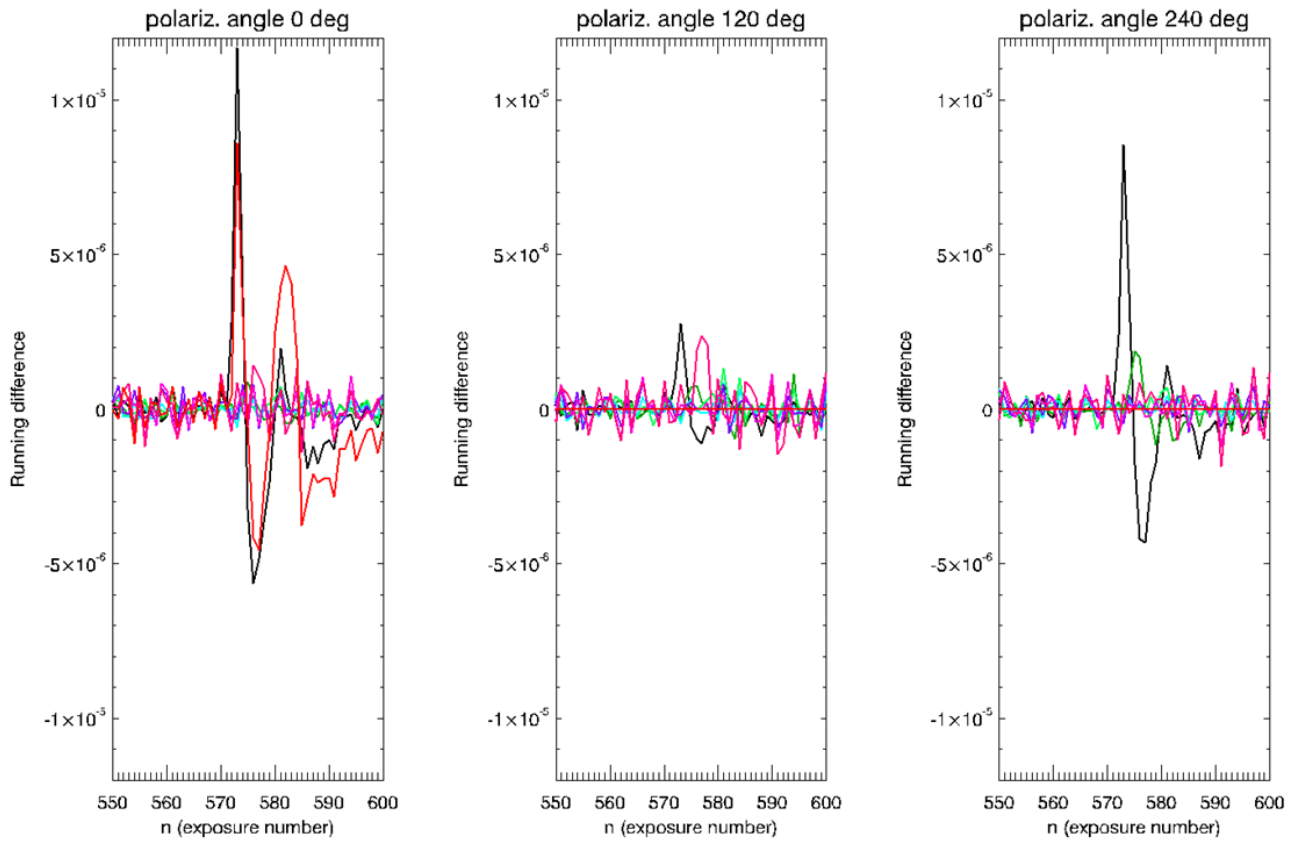

Figure 11: running differences derived in different angular sectors (shown as different colors) by considering exposures acquired with orientation of the linear polarizer equal to 0° (left panel), 120° (middle panel) and 240° (right panel).

As mentioned before, the Metis software will not derive on board the tB and pB values, hence the CME flag has to deal only with intensities measured in exposures acquired with a single orientation of the linear polarizer. Nevertheless, these images will be acquired with 4 different orientations (0°, 45°, 90° and 135°) and this opens the following problem: which one of these sequences will be employed to produce the flag? This problem is not trivial, as shown by a comparison (Figure 11) between running differences derived with exposures acquired with the 3 different polarization angles (0°, 120° and 240°) available from STEREO-COR1 data. Figure 11 shown that the definition of a single threshold value for the running differences depends on the considered orientation of the polarizer, making hard to define a single threshold value even for a single event. Running difference values are maxima for exposures acquired at 0° (left panel), minima with exposures at 120° (middle panel), and intermediate with exposures at 240° (right panel).

The physical explanation for the above results is the following: due to Thomson scattering, the polarization vector is always tangent to the solar limb, and the same applies for plasma embedded in CMEs. Hence, in single images acquired with a specific orientation of polarization angle the CME intensity will be more or less attenuated, depending on the angle θ_{CME} between the CME and the orientation of the polarizer. In particular, the CME intensity will be maximum when the angle between the CME central latitude and the orientation of the polarizer will be closer to θ_{CME} = 90° $\pm$ 180°, and minimum when this angle will be closer to θ_{CME} = $\pm$ 180°. As a consequence, the visible light peak intensity of a CME (hence the peak in running differences) strongly depends on that angle: this means that exposures acquired with a single orientation of the polarizer are not suitable for the implementation of a CME flag.

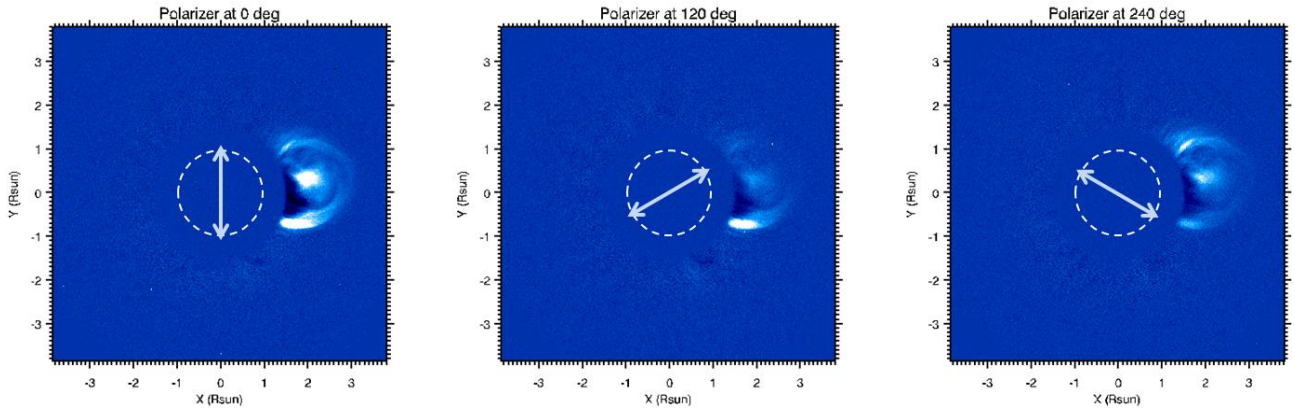

Figure 12: VL intensities observed during the CME by STEREO COR1 (pre-CME corona subtracted) with the linear polarizer oriented at 0° (left panel), 120° (middle panel) and 240° (right panel) with respect to the solar north. The range of color scale is the same for the three panels shown here (from -100 to +100).

This very important point is better shown in Figure 12, where the VL intensities observed for the same event with 3 different orientations of the linear polarizer are provided. This Figure also shows clearly that the CME intensity increases moving toward angles closer to the condition θ_{CME} = 90° $\pm$ 180°, making also the identification of CME central latitude very uncertain.

A possible quick solution to this problem could be provided by the following reasoning: because in each image acquired with single orientation angle θ_{pol} of the linear polarizer, the CME intensity will maximize in coronal regions located around angles of θ_{pol} $\pm$ 90° (as shown in Figures 11 and 12), running differences

should be built according to this fact. Hence, the 8 elements of the intensities (hence of the running difference values Δ_i) should be computed with the selection rule given in Table 1.

Vector element number	Angular interval for the average (measured from the solar west)	Image (orientation of polarizer measured from the solar north)
0	-22.5° – +22.5°	Polarizer at 0°
1	+22.5° – +67.5°	Polarizer at 45°
2	+67.5° – +112.5°	Polarizer at 90°
3	+112.5° – +157.5°	Polarizer at 135°
4	+157.5° – +202.5°	Polarizer at 0°
5	+202.5° – +247.5°	Polarizer at 45°
6	+247.5° – +292.5°	Polarizer at 90°
7	+292.5° – +337.5°	Polarizer at 135°

Table 1: suggested selection rule for latitudinal regions of Metis images where the signal has to be added in order to compute the running differences for the CME flag depending on the orientation of the linear polarizer. This is the selection rule suggested when pB measurements are performed.

The same selection rule is also shown in Figure 13, where for each one of the 4 possible orientations (0°, 45°, 90° and 135°) of the Metis linear polarizer (given by white arrows) the locations of the coronal regions where pixels have to be summed to build the average intensities $I_i(\vartheta_n)$ are filled with red color. With this rule for each sequence of 4 polarized images the 8-element array of intensities summed over 8 different angular sectors will be built. Then by taking the differences $\Delta_i(\vartheta_n) = I_{i+1}(\vartheta_n) - I_i(\vartheta_n)$ the 8-element array of running differences evaluated over different sectors will be built. Hence, by imposing that each angular sector is always centered at an angle of $\pm$ 90° from the orientation of the linear polarizer the problem of CME intensity variations depending on the angle θ_{CME} will be minimized.

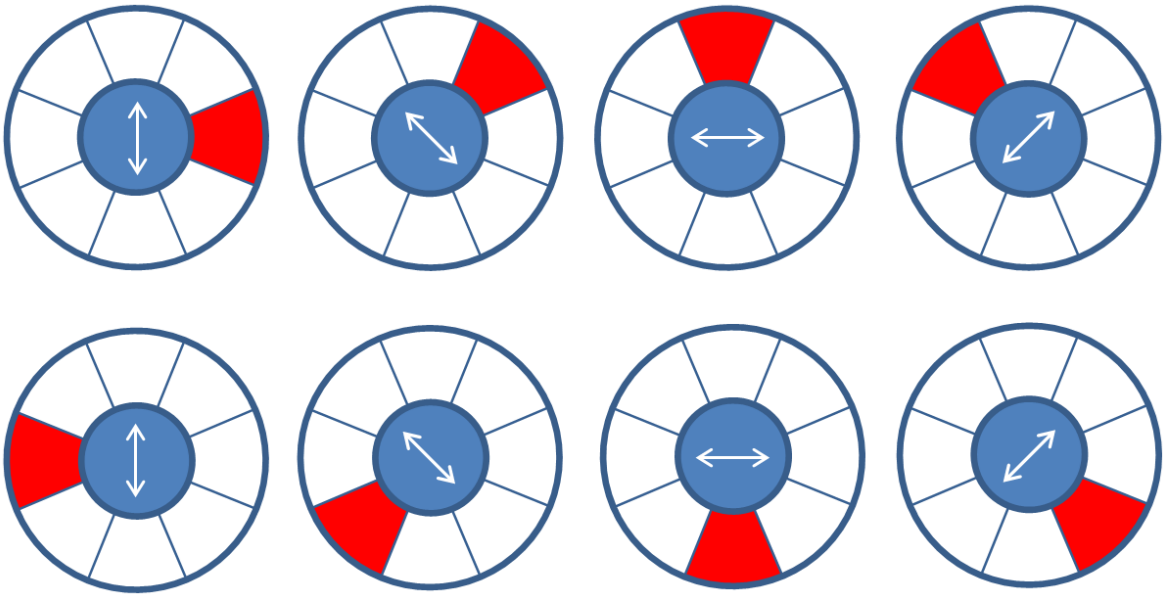

Figure 13: locations of the coronal sectors (red color) where pixels of the Metis images will be summed depending on the orientations (white arrows) of the linear polarizer. This is the selection rule suggested when pB measurements are performed.

In order to test the real improvement given by the solution suggested above, STEREO COR1 data have been analyzed again: because these data are acquired only with 3 polarization angles (0°, 120° and 240°), the

number of angular sectors has been reduced from 8 to 6, as shown in Figure 7 (right panel). The intensity of each sector has been summed from the image acquired with the orientation of the linear polarizer at $\pm$ 90° from the center of the considered sector. Resulting running differences obtained in different angular sectors are shown in Figure 14 (to be compared with plots in Figure 11). Plots in Figure 14 clearly show that, by selecting for instance a threshold corresponding to a relative intensity increase $\Delta_i(\vartheta_n)/I_i(\vartheta_n)$ by about ~ 0.2% – 0.3%, the occurrence of the CME could be unambiguously identified, together with the CME central latitude, thus fulfilling the first two requirements from the flag mentioned in the Introduction. With a relative threshold value of 0.2% the flag will be activated on 1 of the 6 angular sectors, thus allowing the identification of the CME as a regular (and not a halo) event.

The general validity of these values for the threshold of running difference will be better verified in the future by analyzing many more events. In any case, I also point out that in order to reduce any possible uncertainty for the definition of a threshold associated with the instrument calibration, it is also strongly suggested to use the relative (and not absolute) variations of VL running differences $\Delta_i(\theta_n)/I_i(\theta_n)$.

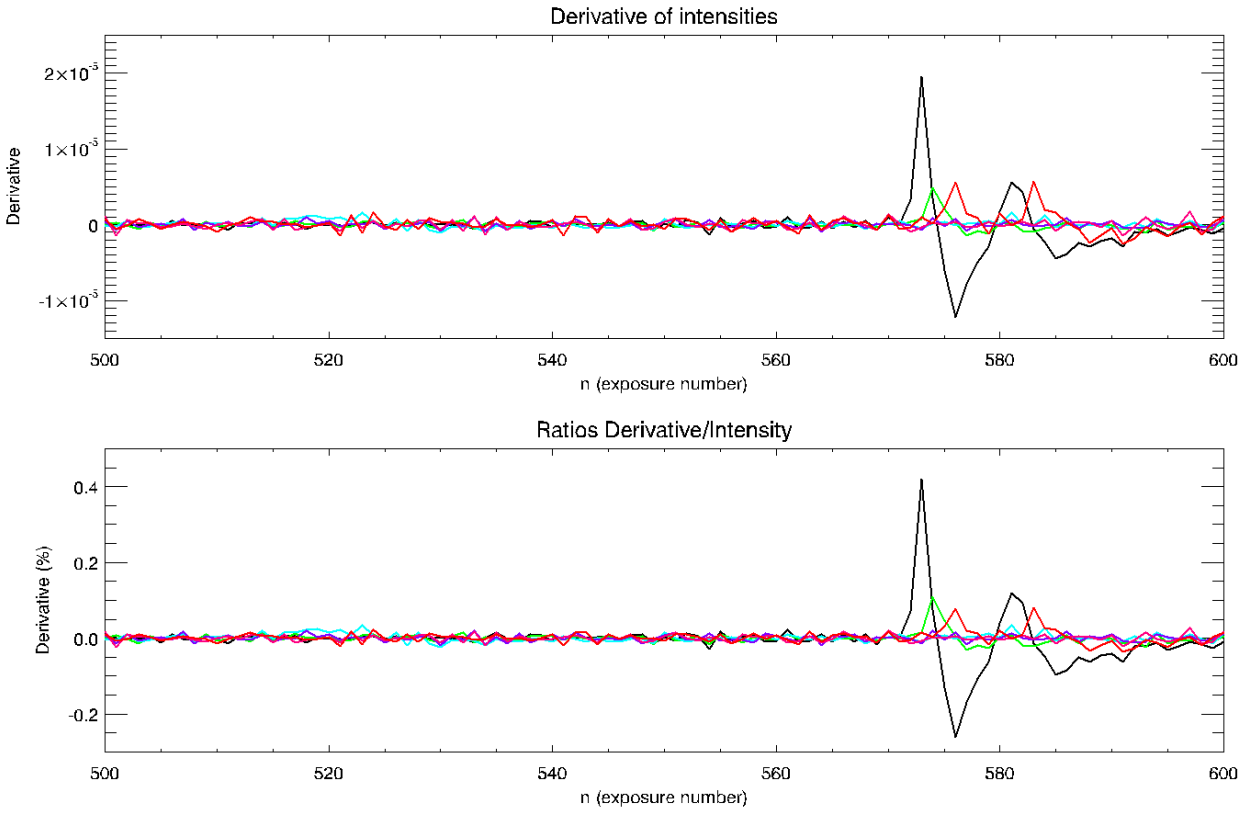

Figure 14: absolute (top) and relative (bottom) values of running differences for the standard CME built in different angular sectors (different colors) with the rule explained in the text for the selection of polarized images.

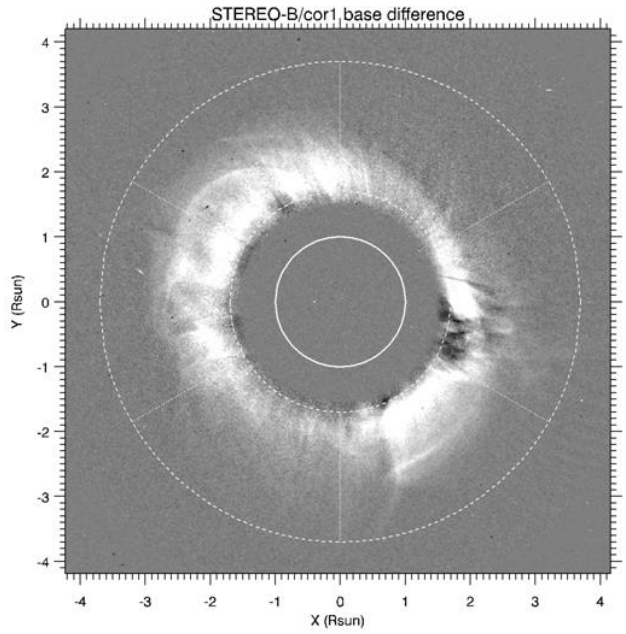

Figure 15: total brightness (pre-CME image subtracted) observed in the exposure where the halo CME intensity maximizes, together with the considered 6 angular sectors (dotted lines). This Figure shows that all the angular sectors were involved in the eruption.

In other cases Metis instrument will acquire sequences of images only with 2 orientations of the linear polarizer (at 0° and 90° with respect to the north pole) in order to perform measurements of tB and not of pB. The more simple (and computationally quicker) solution is to replace the 2 missing exposures acquired with the polarizer at 45° and 135° with an average between 2 images acquired at 0° and 90°. In this way, possible underestimates of CME intensities due to polarization will be minimized. Hence, the selection rule in this case is given in Table 2 and shown in Figure 16.

Vector element number	Angular interval for the average (measured from the solar west)	Image (orientation of polarizer measured from the solar north)
0	-22.5° – +22.5°	Polarizer at 0°
1	+22.5° – +67.5°	Average between polarizer at 0° and 90°
2	+67.5° – +112.5°	Polarizer at 90°
3	+112.5° – +157.5°	Average between polarizer at 0° and 90°
4	+157.5° – +202.5°	Polarizer at 0°
5	+202.5° – +247.5°	Average between polarizer at 0° and 90°
6	+247.5° – +292.5°	Polarizer at 90°
7	+292.5° – +337.5°	Average between polarizer at 0° and 90°

Table 2: suggested selection rule for latitudinal regions of Metis images where the signal has to be added in order to compute the running differences for the CME flag depending on the orientation of the linear polarizer. This is the selection rule suggested when tB measurements are performed.

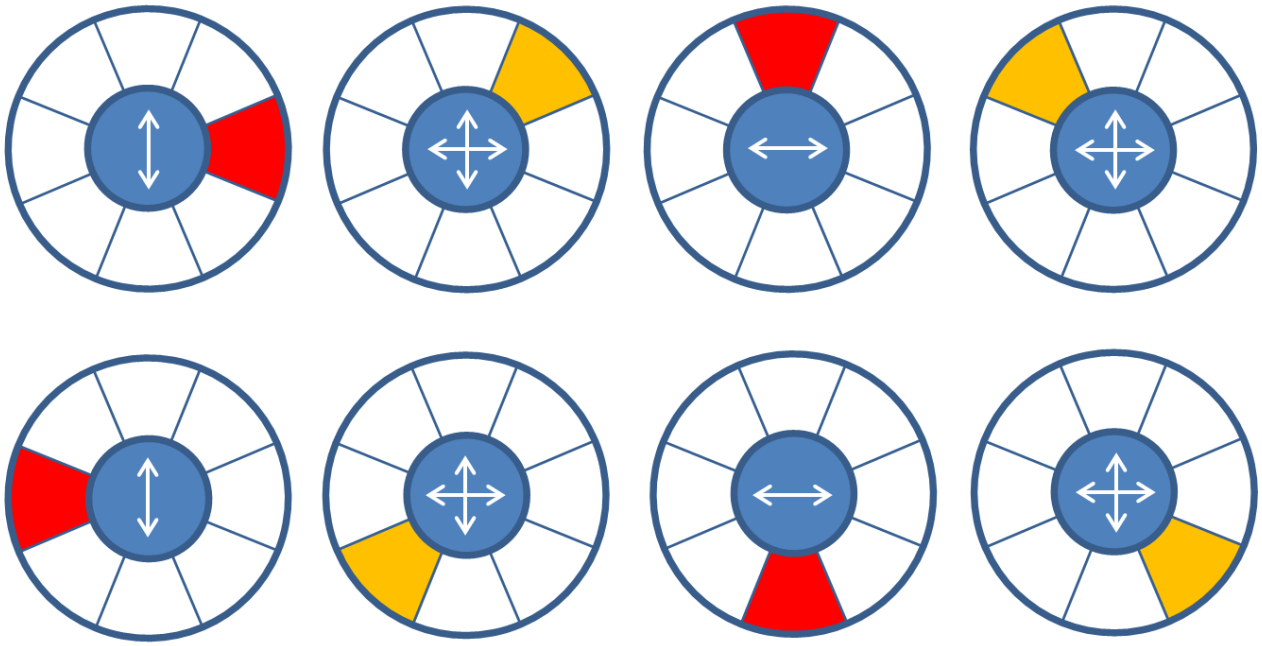

Figure 16: locations of the coronal sectors where pixels of the Metis images will be summed (red color) or averaged between 2 images (orange color) depending on the orientations (white arrows) of the linear polarizer. This is the selection rule suggested when tB measurements are performed.

7. Test for a Halo CME flag

The halo CME selected for this first test is shown in Figure 6 as a sequence of regular (left) and running difference (right) images, as well as in Figure 15 as a single base difference image (last image before the CME subtracted, as done for Figure 8). The same analysis described above for the CME flag test has been repeated with the 321 images (corresponding to 107 triplets of polarized exposures) considered for this event. The intensity and running difference arrays have been built again by summing all the pixels over 6 angular sectors, by extracting the intensity for each sector in the image acquired with an orientation of the linear polarizer perpendicular to the central location of the angular sector, with the selection rule described above.

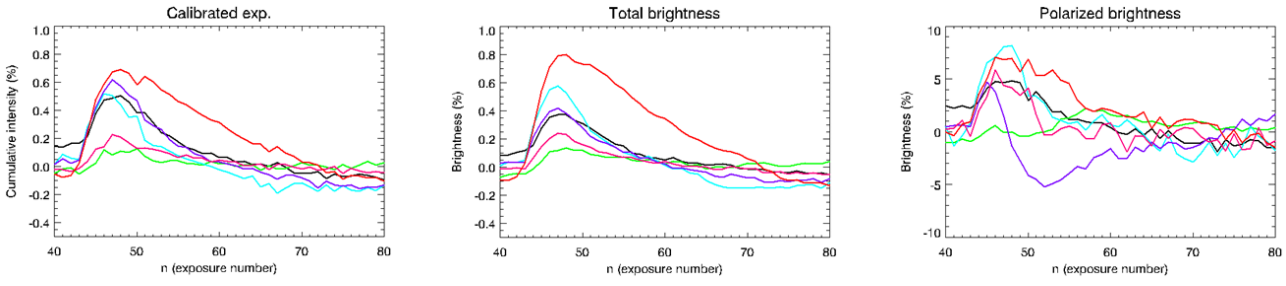

Figura 17: evolution of the intensities (relative variations in %) in different angular sectors (shown with different colors) computed by averaging the signal measured in exposures with single orientation of the linear polarizer (left panel, 0°), total brightness (middle) and polarized brightness (right). This Figure can be directly compared with Figure 9.

Resulting curves for the relative variations (%) of the intensity measured in images with single orientation of the polarizer (0°), total brightness tB and polarized brightness pB are shown in Figure 17. The main results from this analysis can be summarized as follows:

- Brightness in images acquired with single polarization angle (left) and total brightness tB (middle) increase by the same order than what observed for the standard CME.
- Increase of the total brightness tB is much smoother than what observed for the standard CME (Figure 9), where the tB intensity increase was much more sharp.
- Variation of the polarized brightness pB is much smaller than what observed for the standard CME (Figure 9), where the pB intensity increase was much stronger (in %).

The smoother intensity increase is likely due to projection effects expected for halo CMEs, which are expanding towards the observer. The smaller fraction of polarized light observed is in agreement with the fact that the fraction of pB decreases as one moves away from the plane of the sky, and the plasma embedded in halo CMEs is in fact located much farther from that plane, because the eruption is expanding towards the observer. Hence, the problem described above for the standard CME in the selection of the angle of polarization to be used to build the intensity and running difference arrays will be less important for halo CMEs.

The corresponding evolution of running differences in considered 6 angular sectors is shown in Figure 18: for a direct comparison with running differences observed for the standard CME, curves in this Figure are plotted with the same scale of the vertical axis. Figure 18 shows that the peak values of running differences are about a factor ~3 smaller than what observed for the standard CME: this difference is not due to the peak intensity of the CME (Figure 17), but to the much smoother transition during the intensity increase.

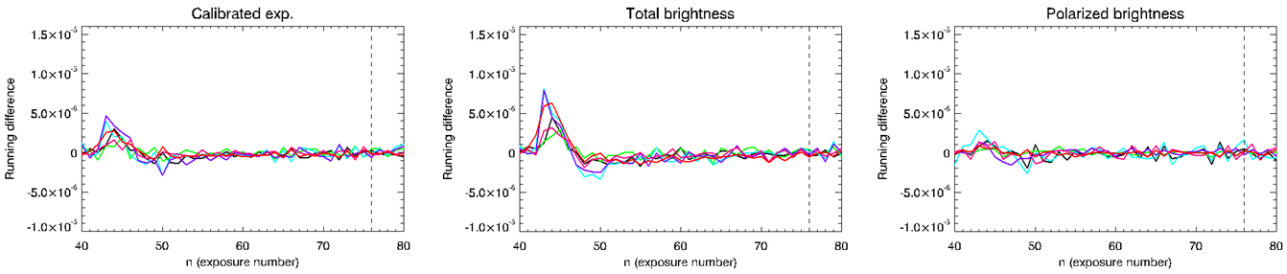

Figure 18: evolution of running difference signals Δ_i over a subset of the whole observation interval considered here (12 hours of data); different colors represent different angular sectors. For a direct comparison, the vertical axes in the plots have the same scale used for plots in Figure 10.

Hence, the implementation of a halo flag will require the selection of a much smaller value for the threshold: in particular Figure 19 shows the absolute (top) and relative (bottom) variations of running differences obtained with the selection rule explained above for the selection of polarized images (each angular sector is always centered at an angle of $\pm$ 90° from the orientation of the linear polarizer). These plots show that for the activation of a halo flag it will be necessary to select a smaller relative threshold value around $\Delta_i(\vartheta_n)/I_i(\vartheta_n)$ ~ 0.1% – 0.15%. With a relative threshold value of 0.1% the flag will be activated on 4 of the 6 angular sectors, thus allowing the identification of the CME as a halo (and not a regular) event.

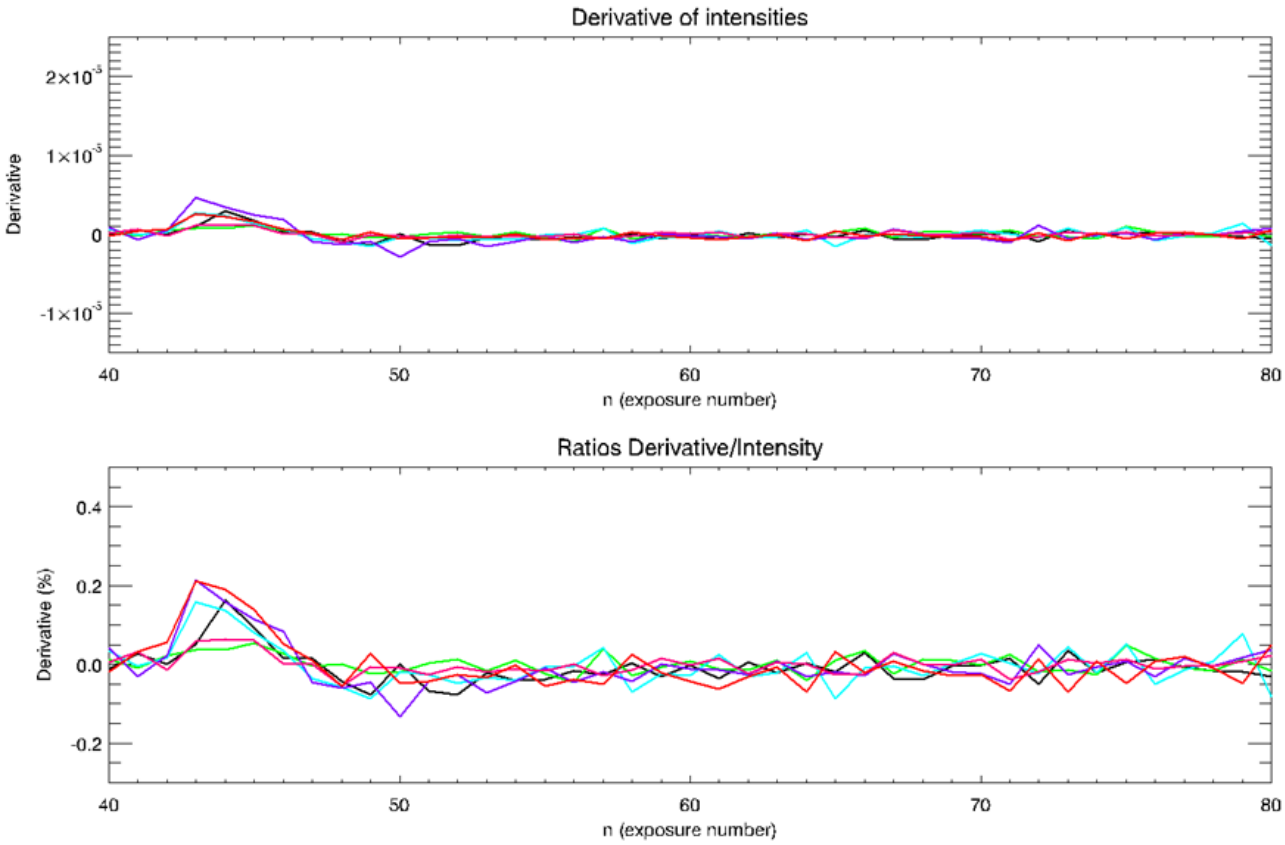

Figure 19: absolute (top) and relative (bottom) values of running differences for the halo CME built in different angular sectors (different colors) with the rule explained in the text for the selection of polarized images. For a direct comparison, the vertical axes in the plots have the same scale used for plots in Figure 14.

The general validity of these values for the threshold of running difference will be better verified in the future by analyzing many more events. The future analysis will investigate other topics like:

- the effects of a different radial extension of the coronal region employed for the computation of averages in different angular sectors,
- how the implementation of a threshold for the CME flags could be affected by the plasma expansion as the Solar Orbiter spacecraft will observe these events from different heliocentric distances along its orbit,

and other effects.